Power deposition in the head and neck of an anatomically based human body model for plane wave exposures

1998 Phys. Med. Biol. 43 2361

(http://iopscience.iop.org/0031-9155/43/8/026)

Phys. Med. Biol. **43** (1998) 2361–2378. Printed in the UK PII: S0031-9155(98)86746-8

Power deposition in the head and neck of an anatomically based human body model for plane wave exposures

A D Tinniswood, C M Furse and O P Gandhi

Department of Electrical Engineering, University of Utah, Salt Lake City, UT 84112, USA

Received 11 August 1997, in final form 29 January 1998

Abstract. At certain frequencies, when the human head becomes a resonant structure, the power absorbed by the head and neck, when the body is exposed to a vertically polarized plane wave propagating from front to back, becomes significantly larger than would ordinarily be expected from its shadow cross section. This has possible implications in the study of the biological effects of electromagnetic fields. Additionally the frequencies at which these resonances occur are not readily predicted by simple approximations of the head in isolation. In order to determine these resonant conditions an anatomically based model of the whole human body has been used, with the finite-difference time-domain (FDTD) algorithm to accurately determine field propagation, specific absorption rate (SAR) distributions and power absorption in both the whole body and the head region (head and neck). This paper shows that resonant frequencies can be determined using two methods. The first is by use of the accurate anatomically based model (with heterogeneous tissue properties) and secondly using a model built from parallelepiped sections (for the torso and legs), an ellipsoid for the head and a cylinder for the neck. This approximation to the human body is built from homogeneous tissue the equivalent of two-thirds the conductivity and dielectric constant of that of muscle. An IBM SP-2 supercomputer together with a parallel FDTD code has been used to accommodate the large problem size. We find resonant frequencies for the head and neck at 207 MHz and 193 MHz for the isolated and grounded conditions, with absorption cross sections that are respectively 3.27 and 2.62 times the shadow cross section.

1. Introduction

Previous work by Gandhi *et al* (1992) and Stuchly *et al* (1988) has investigated power dissipation in the human body (for both isolated and grounded conditions), giving results for power absorbed in many of the internal organs. Whereas coarser resolutions were used in the above works, in the present work a higher-resolution anatomically based model, the so-called 2 mm model of the human body, has been used with a resolution of 1.974 mm in the cross-sectional planes (δ_x, δ_y) and 3.0 mm in the vertical dimension (δ_z). This model has been derived from magnetic resonance imaging (MRI) scans of a male volunteer, which have been classified into a number of different tissues. The computational and storage requirements for finite-difference time-domain (FDTD) simulation using this high-resolution model prohibited its use for a large number of simulations. A lower-resolution model, the so-called 6 mm model, with a cell size of δ_x and δ_y equal to 5.922 mm and δ_z equal to 6.0 mm, has therefore been developed by combining the cells of the higher-resolution model. A $3 \times 3 \times 2$ cell combination has been used, with the majority tissue in each of

0031-9155/98/082361+18$19.50

these combination volumes being assigned as the value in the lower-resolution model. This model, which is a factor of 18 times smaller than the higher-resolution model, allows much faster simulations. Therefore simulations can be carried out for more frequencies. The higher-resolution model, which required a parallel supercomputer for simulation, was used when the resonant frequencies had been found. The size (in voxels) and weights of the individual organs in both the high- and low-resolution models are given in table 1 which also compares these with those given for reference man (IRCP 1975). It should be noted that as the outer parts of the arms were outside the field of view of the MRI scanner these regions are missing for this model.

Table 1. Weights of individual tissues in the two anatomically based models of the human body.

Tissue	Mass density (g cm^{-3})	Weight (6 mm model)	Weight (2 mm model)	Reference man
Muscle	1.047	32.25 kg	31.87 kg	28.0 kg
Fat	0.916	15.98 kg	14.86 kg	13.5 kg
Bone[a]	1.465	10.98 kg	10.98 kg	10.0 kg
Cartilage	1.097	180.0 g[b]	175.4 g[b]	2.5 kg
Skin[c]	0.983	2.93 kg	3.26 kg	2.6 kg
Nerve	1.038	59.6 g[d]	65.7 g[d]	30.0 g[e]
Intestine	1.042	1.35 kg[i]	1.27 kg[i]	1.01 kg[j]
Pancreas	1.045	119 g	114.8 g	100.0 g
Heart	1.030	714 g[i]	713.1 g[i]	450.0 g[j]
Blood	1.058	739 g[f]	718.3 g[f]	5.5 kg
Liver	1.030[h]	1.85 kg	1.76 kg	1.8 kg
Kidney[g]	1.050	317 g	304.0 g	310.0 g
Lung[g]	0.347	1.039 kg	983.8 g	1.0 kg
Bladder	1.030	234 g[i]	217.4 g[i]	150-250 g
Stomach	1.050	637 g[i]	588.1 g[i]	150.0 g[j]
Prostate gland	1.045	38.1 g	34.5 g	16.0 g
Testicle[g]	1.044	96.3 g	88.1 g	60.0 g
Ligament	1.220	425.5 g	418.2 g	1.5 kg
Brain	1.048	1.75 kg	1.67 kg	1.40 kg
Pineal gland	1.066	0.23 g	0.23 g	0.18 g
Pituitary gland	1.035	0.23 g	0.28 g	0.6 g

[a] Compact and regular bone combined.
[b] Major cartilage regions (ears, nose) only. No bone-end cartilage.
[c] One-voxel thick layer around entire body except eyes and ear canal.
[d] Spinal cord, optic nerve, other large nerves included.
[e] Spinal cord only.
[f] Major arteries and vessels only.
[g] Pair.
[h] No value given. Estimate bases on tissue content.
[i] Full (contents are not differentiated from organ).
[j] Empty (organ only).

Figure 1 shows a three-dimensional image of the anatomically based whole body model used. For the power absorption in the head and neck we have taken the total power absorbed in the first 42 or 84 layers (for the lower- and higher-resolution models respectively), or alternatively the top 25.2 cm of the model. The effective cross-sectional area gives a measure of the conduction through each layer of the model, and is a metric used in Gandhi *et al* (1992). As the effective cross section is a function of the conductivity at each point on the cross section, it is also a frequency-dependent parameter. The effective cross section

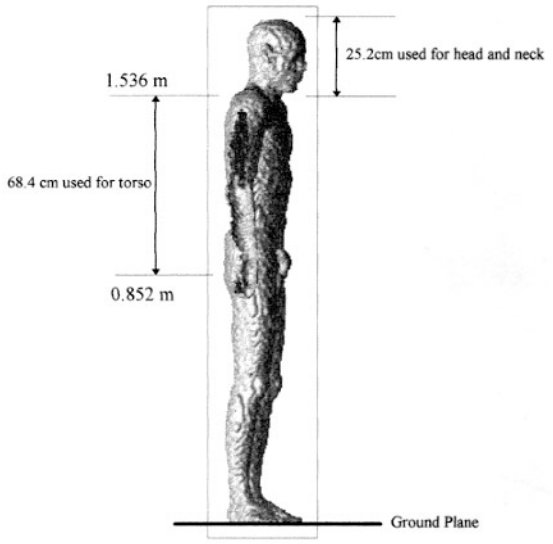

Figure 1. A 3D image showing the anatomically based model of the human body, with the top 25.2 cm being taken as the head and neck region. For grounded simulations a ground plane is placed immediately below the feet of the model, which have been flattened for this purpose.

(equation (1)) of this model at 193 MHz is shown in figure 2.

$$A_{\mathrm{eff}}(k) = \sum_{j=1}^{N_j} \sum_{i=1}^{N_i} \frac{\sigma(i, j, k)\delta_x \delta_y}{\sigma_{2/3\,\mathrm{muscle}}} \tag{1}$$

where A_{eff} is the effective cross section for slice k, $\sigma(i, j, k)$ is the conductivity in the model at point (i, j, k) and $\sigma_{2/3\,\mathrm{muscle}}$ is two-thirds the conductivity of muscle.

Of interest in this paper is the power absorbed in the head and neck and the frequencies at which it is maximum, the so-called 'resonant frequencies'. The enhancement factor S (equation (2)) is a dimensionless quantity which provides a measure of the effective cross section of the head:

$$S = \frac{A_{\mathrm{Abs}}}{A_{\mathrm{shadow}}} \tag{2}$$

where A_{Abs} is the effective absorption cross section given by $P_{\mathrm{Abs}}/D_{\mathrm{inc}}$, with P_{Abs} being power absorbed (W), and D_{inc} the incident power density (W m^{-2}) of the plane wave. A_{shadow} is the shadow cross-sectional area (m^2) of the head. The shadow cross section of the head and neck together with the weights of the whole model and head and neck alone are given in table 2.

Additional consideration has been made for children aged 10 and 5 years, being exposed to similar electric fields. Simulations using a scaled version of the man model have been carried out over the same frequency range as the adult male runs. The cell sizes used in these models are δ_x, $\delta_y = 4.53$ mm and $\delta_z = 3.8967$ mm and δ_x, $\delta_y = 4.6938$ mm and $\delta_z = 3.8096$ mm, for the 10- and 5-year-old child respectively. The weight of the 10-year-old child was 33.7 kg, with the head and neck weight being 2.75 kg. The weight of the 5-year-old child was 20.26 kg, with the head and neck weight being 1.26 kg. These weights agree with the corresponding weights of 33 kg and 21 kg given in reference man (IRCP 1975) for children of similar ages. Again the shadow cross sections of the head and

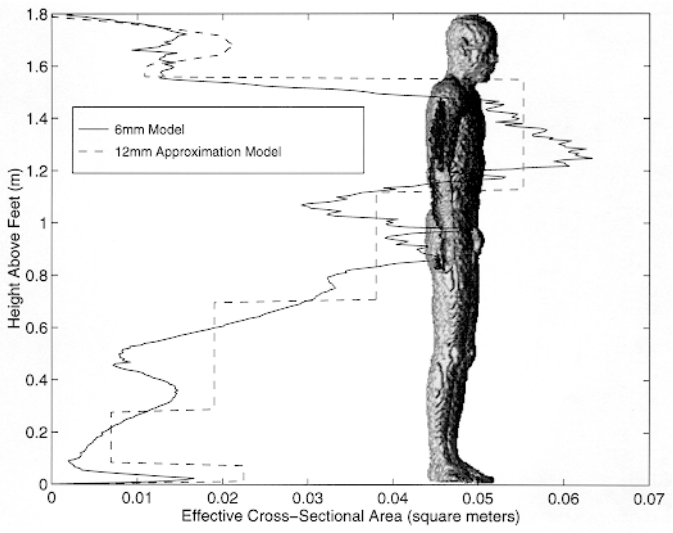

Figure 2. The effective cross section of the 6 mm whole body model at 193 MHz. Also shown by the broken line is the effective cross section assumed for the 12 mm rectangular approximation model used for the calculations.

Table 2. The shadow cross-sectional area, and the head and whole body weights of the original 2 mm whole body model, the 6 mm whole body (adult, 10- and 5-year-old children) models and the 12 mm cube approximation model.

	2 mm model (adult)	6 mm model (adult)	Scaled model (10-year-old child)	Scaled model (5-year-old child)	12 mm cube approximation
Head and neck shadow cross sectional area (m^2)	0.0355	0.0366	0.0208	0.0154	0.0372
Whole body shadow cross sectional area (m^2)	0.508	0.516	0.305	0.213	0.401
Head weight (kg)	5.39	5.26	2.75	1.66	5.16
Whole body weight (kg)	69.84	70.88	33.70	20.26	81.46
Height (m)	1.80	1.80	1.41	1.41	1.80

neck together with the whole body and head and neck weights of the scaled child models are given in table 2.

2. The simulation method

The use of the FDTD algorithm, which is the method of choice for bioelectromagnetic simulations, is discussed in many publications, but the book by Taflove (1995) covers the subject most thoroughly. A parallel implementation of the FDTD algorithm (Tinniswood

et al submitted) has been used to generate the results in this paper, which in combination with a high-power parallel supercomputer (such as the IBM SP2) can accommodate extremely large problem sizes. The simulation size and execution times using the parallel FDTD code, with both the high- and low-resolution whole body models are given in table 3.

Table 3. Size and execution time of the higher- and lower-resolution anatomically based heterogeneous whole body models used in this work.

	6 mm man model	2 mm man model
Model size (voxel)	1 275 000	23 580 160
FDTD problem size (cells)	2 289 144	28 987 556
Memory requirement	60.5 MBytes	765.6 MBytes
Solution time on workstation[a]	2.3 hours	87.3 hours (estimated)[b]
Solution time on 8 IBM SP-2 nodes[a]	19.6 minutes	15.2 hours
Solution time on 16 IBM SP-2 nodes[a]	10.3 minutes	8.0 hours
Solution time on 32 IBM SP-2 nodes[a]	7.0 minutes	4.3 hours

[a] These times are for 100 MHz simulation with 4000 time steps at 6 mm resolution and 8000 time steps at 2 mm resolution. At lower frequencies more time steps are required (as we run for four cycles) and at higher frequencies fewer time steps are required.
[b] There is not enough memory on the available workstation to run this simulation.

Following the information and results of the work previously carried out by our group (Gandhi *et al* 1992), we ran simulations for frequencies from 10 MHz to 350 MHz, in 10 MHz intervals. Although the $(FD)^2TD$ (frequency-dependent finite-difference time-domain) method could have been used, successful results have previously been achieved using sinusoidal excitation. Additionally, in order to get organ-averaged SARs for each of these frequencies, the amount of information required by the $(FD)^2TD$ method becomes prohibitively large. The whole body human model was subject to plane wave exposure, in both grounded and isolated conditions for vertically polarized incident E-fields. The FDTD method has been shown to give accurate results providing certain criteria are maintained. The first is that the ratio of the cell size with respect to wavelength is observed, in that there should be at least 10 cells per wavelength throughout the model. It has, however, been shown that for layer-averaged quantities (e.g. layer-averaged SAR (specific absorption rate) and layer currents) four cells per wavelength is adequate (Gandhi *et al* 1992). At 350 MHz, the highest frequency used in this paper, the wavelength in the brain (one of the tissues in the body with the highest dielectric constant and thus the shortest wavelength), is 12.2 cm. This means that the cell size of 5.922 mm is more than adequate for the frequency range discussed. A second consideration which must be addressed is the number of iterations for which the FDTD technique must be run before we can consider the system as being stable. It has been shown, again in the work done by this group (Gandhi *et al* 1992), that four cycles is adequate for this purpose. Care must also be taken to leave enough space around the model, between the model and the outer boundaries, so that the reflections from the numerical boundary conditions are minimized. Earlier work carried out in this laboratory (Gandhi *et al* 1992) has shown that an extra 10 cells surrounding the model is sufficient for most of the simulations we discuss in this paper.

In the FDTD simulation the model of the human body describes the positions of various organs within the human body. It is, however, necessary to have dielectric properties for each of these tissues. Although many measurements have been made over a wide range of frequencies, not all the frequencies we have used have directly measured tissue properties readily available. However, a wide range of tissue properties have been measured by Gabriel (1996). She has also generated Cole–Cole coefficients to allow tissue properties to be found for a wide range of frequencies. It is these tissue properties which we have used and a selection of them is given in table 4.

Table 4. Tissue properties used at 10 MHz, 100 MHz, 200 MHz and 300 MHz. These properties were obtained using the Cole–Cole parameters given by Gabriel [6]. σ has the units of S m^{-1}.

	10 MHz		100 MHz		200 MHz		300 MHz	
Tissue	ε_r	σ	ε_r	σ	ε_r	σ	ε_r	σ
Muscle	170.73	0.62	65.97	0.71	60.23	0.74	58.2	0.77
Fat	21.68	0.04	9.39	0.05	8.86	0.06	8.69	0.06
Bone	36.03	0.07	10.39	0.09	9.29	0.10	8.95	0.10
Cartilage	179.28	0.37	55.76	0.47	49.16	0.52	46.77	0.55
Skin	291.74	0.28	69.45	0.51	55.69	0.58	50.86	0.64
Nerve	155.07	0.22	47.26	0.34	39.71	0.38	36.91	0.42
Intestine	488.46	1.34	96.55	1.66	76.71	1.77	69.77	1.84
Spleen	440.51	0.51	90.66	0.80	72.74	0.90	66.49	0.97
Pancreas	440.51	0.51	90.66	0.80	72.74	0.90	66.49	0.97
Heart	199.80	0.96	85.89	1.07	74.20	1.13	70.27	1.16
Blood	280.09	1.10	76.82	1.23	68.48	1.28	65.65	1.32
Parotid gland	247.68	0.23	68.47	0.44	56.06	0.51	51.90	0.55
Liver	223.12	0.32	69.02	0.49	57.72	0.56	53.51	0.61
Kidney	371.15	0.51	98.09	0.81	78.00	0.94	70.48	1.02
Lung	123.66	0.23	31.64	0.31	26.58	0.34	24.77	0.36
Bladder	51.50	0.27	22.65	0.29	20.79	0.31	20.09	0.32
CSF	108.59	2.00	88.90	2.11	76.82	2.19	72.73	2.22
Humour	70.01	1.50	69.80	1.50	69.04	1.51	69.02	1.52
Sclera	208.20	0.80	67.88	0.90	61.23	0.94	58.90	0.98
Lens	137.20	0.37	50.01	0.45	45.26	0.48	43.65	0.50
Stomach	246.43	1.34	77.90	1.66	71.04	1.77	68.71	1.84
Prostate gland	246.93	0.78	75.60	0.91	67.61	0.96	64.84	0.99
Testicle	246.93	0.78	75.60	0.91	67.61	0.96	64.84	0.99
Ligament	103.21	0.41	53.92	0.49	49.37	0.52	47.98	0.54
Pineal gland	247.68	0.23	68.47	0.44	56.06	0.51	51.90	0.55
Pituitary gland	247.68	0.23	68.47	0.44	56.06	0.51	51.90	0.55
Brain	247.68	0.23	68.47	0.44	56.06	0.51	51.90	0.55

As has been stated, this work has focused on the absorption of power in the human head and neck. However, it is not possible to draw conclusions about the head absorption spectrum from simulations using an isolated head and neck model. This absorption spectrum is greatly modified by the presence of the rest of the human body. We will therefore present some results concerning the SAR distribution in the whole of the human body, under both grounded and ungrounded conditions.

The grounded condition is simulated with the FDTD technique by setting the tangential E-fields on all of the cells below the feet of the model to zero. Although many boundary conditions are available, the retarded time boundary conditions (Berntsen and Hornsleth

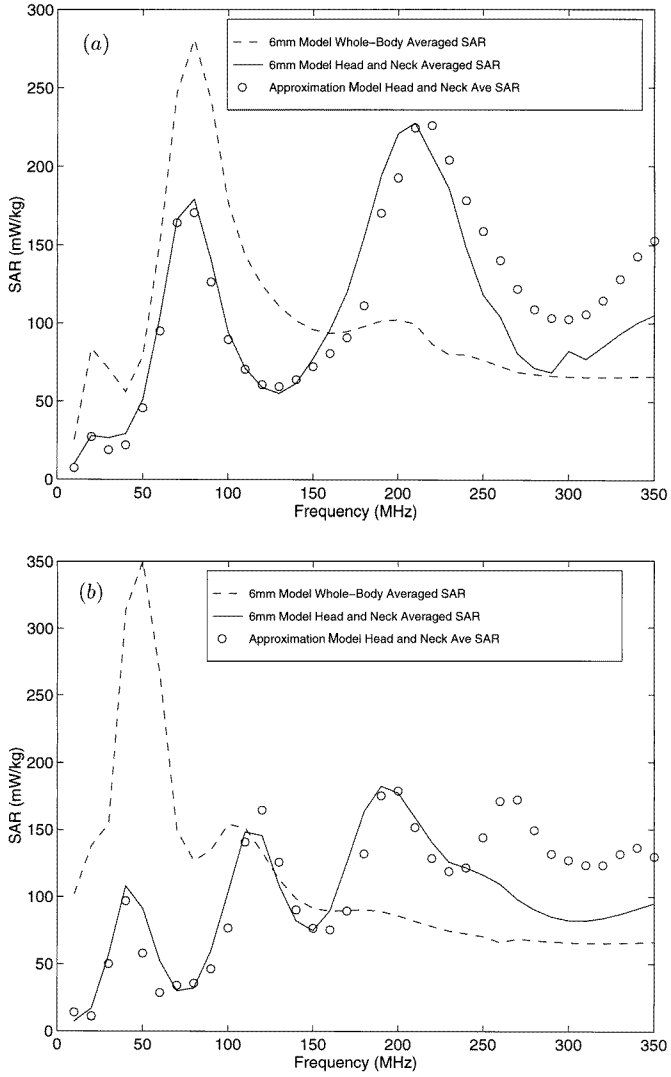

Figure 3. A comparison of the mass-averaged SAR in the head and neck and whole body for an isolated (*a*) and grounded (*b*) heterogeneous 6 mm adult model. Also shown is the mass-averaged SAR for the head and neck of the 12 mm approximation model $D_{\mathrm{inc}} = 1$ mW cm^{-2}.

1994) have been used for their simplicity and low computational load. Previous work in our group (Furse *et al* 1997) has shown that these boundary conditions perform well at the frequencies discussed here, even when compared with the perfectly matched layer (PML) absorbing boundary conditions.

Simulations using the lower-resolution models were carried out at 10 MHz intervals to establish the approximate position of the resonant frequencies for the head and neck and the whole body. Once these had been found, a 1 MHz interval was chosen to establish these resonant frequencies with greater accuracy. Furthermore a higher-resolution simulation was then carried out at these frequencies in order to achieve more accurate tissue-averaged SAR results.

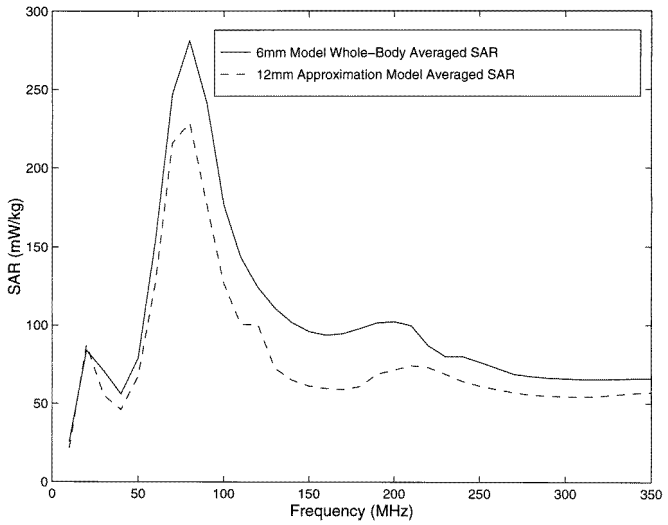

Figure 4. A comparison of the whole-body averaged SAR in the isolated 6 mm heterogeneous anatomically based model and the 12 mm resolution approximation model. $D_{\mathrm{inc}} = 1$ mW cm^{-2}.

3. An approximation model for the human body

An approximation to the effective cross section (figure 2) of the human torso and legs has been built from rectangular sections. For this approximation model the head is represented by an ellipsoid ($a = 9.6$ cm, $b = 10.8$ cm) and the neck by a cylindrical section (length = 3.6 cm) joining this to the torso. The dielectric properties of two-thirds muscle (at the relevant frequency) were used throughout this model. Again the absorption spectrum for this model has been investigated, together with the absorption spectrum of the ellipsoidal and cylindrical region alone (representing the head and neck). The effective cross sections of the 6 mm whole body model and the rectangular approximation model are compared in figure 2. Simulations using this model were carried out over the same frequency range as the 6 mm heterogeneous whole body model. The approximation model is intended to demonstrate that the whole body together with the head and neck resonances are dependent upon the general dimensions and shape of the body and not specific features. The weights of the whole body and the head and neck, together with the shadow cross section of the head, are also given in table 2 for this approximation model. We will demonstrate that a homogeneous two-thirds muscle representation of the body tissues would be quite adequate for the purposes of most of the results presented in this paper. However, the organ-specific SARs would not be possible with the approximation model.

4. Results

All of the SARs given in this paper (figures 3–11 and tables 5 and 6) have been normalized for an assumed incident power density of 1 mW cm^{-2} (10 W m^{-2}). We first present results for whole-body averaged SAR in the isolated (figure 3(*a*)) and grounded (figure 3(*b*)) heterogeneous whole body model, which clearly shows the frequency at which the maximum power absorption occurs. The power absorption in the approximation model was found over

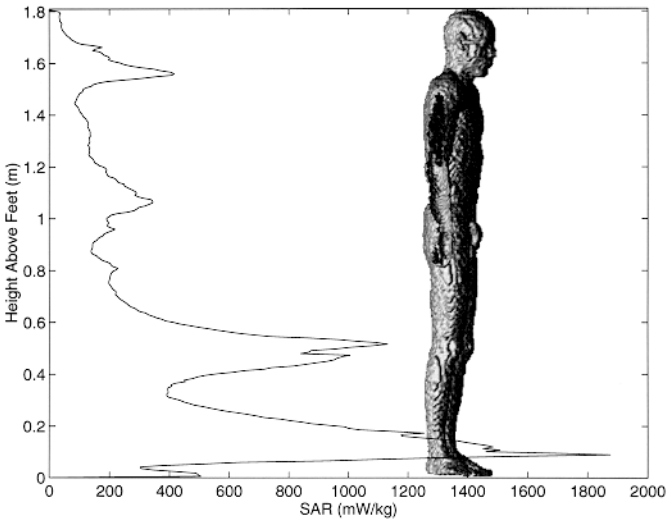

(*a*)

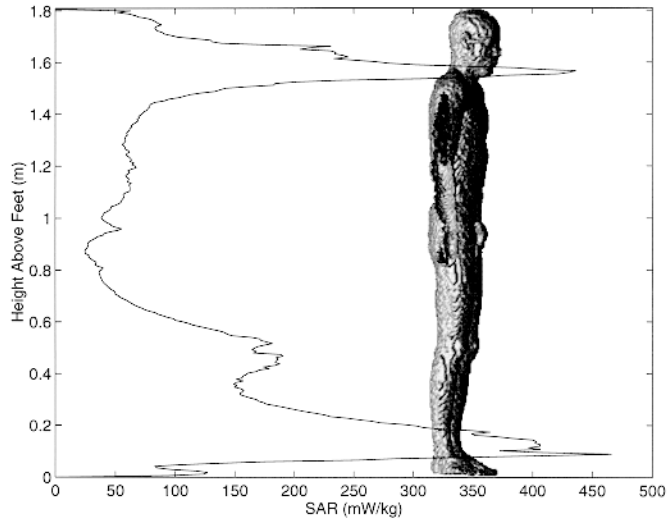

(*b*)

Figure 5. The layer-averaged SAR at 79 MHz (*a*) and 207 MHz (*b*) for the isolated 6 mm whole body man model. $D_{\mathrm{inc}} = 1$ mW cm^{-2}.

a similar frequency range (10–350 MHz) and as expected gives a similar absorption spectrum (figure 4). When observing the fact that the whole-body averaged SAR in the approximation model (at resonance) is less than that of the anatomically based model, the larger mass, but similar shadow cross section, of the former must be considered. It is clear from these results, and particularly the comparisons between the homogeneous approximation model and the heterogeneous anatomically based whole body model, that the absorption spectrum is based upon the general dimensions of the body and not upon specific features within it. Additionally the simplicity of the approximation model lends confidence to this hypothesis.

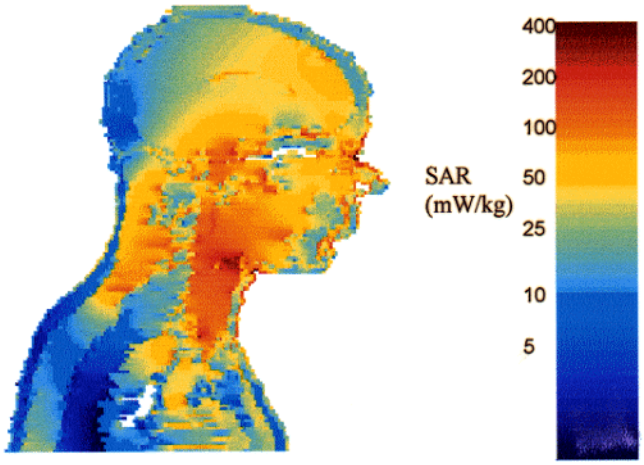

Figure 6. The SAR distribution in the head and neck at 207 MHz under isolated conditions. $D_{\text{inc}} = 1$ mW cm^{-2}.

The whole body resonant frequencies are 79 MHz and 48 MHz respectively for the isolated and grounded model conditions. For whole body absorption conditions, these results show good agreement (in both the resonant frequencies and power absorptions at resonance) with those calculated by Hagmann *et al* (1979) and measured experimentally by Guy *et al* (1984). Our results for whole body resonance also show agreement with those of Dimbylow (1997), where resonance was found at 60 MHz and 35 MHz for isolated and grounded conditions respectively. Dimbylow also found whole-body averaged SARs at resonances of 329 mW kg^{-1} and 360 mW kg^{-1} (for isolated and grounded conditions respectively), which again compare with our values of 282.4 mW kg^{-1} and 357.5 mW kg^{-1}. Although these values are not exactly the same it should be remembered two different human body models were used, and in comparing these two works this needs to be considered.

In this paper we are concerned mainly with the power absorbed in the head and neck of these two models for both isolated and grounded conditions (figures 3(*a*) and 3(*b*) respectively. Again good agreement can be observed between the heterogeneous whole body model and the homogeneous approximation, with the position and magnitude of the resonances being very similar for both cases. Taking first the isolated case (figure 3(*a*)), it is clear that there are two frequencies for which the head and neck are resonant, the first being when the whole body is resonant and the second occurring when the head and neck alone are resonant. It should be noted that the head does not become resonant at a frequency synonymous with using an isolated ellipsoid or sphere as an approximation. The resonant frequency is in fact much lower, at 207 MHz.

From an examination of two-dimension slices through distribution of the SAR in the body at both 79 MHz (whole body resonance) and 207 MHz (head and neck resonance), it has been observed that at 207 MHz the power absorbed is concentrated much more in the head and neck region. This is also clear from the layer-averaged SAR distributions for these same frequencies) figures 5(*a*) and 5(*b*)). Figure 6 provides a closer examination of the SAR distributions in the head and neck region. Clearly from this we can see that the highest absorption is in the neck as the currents generated in the head have to flow into the

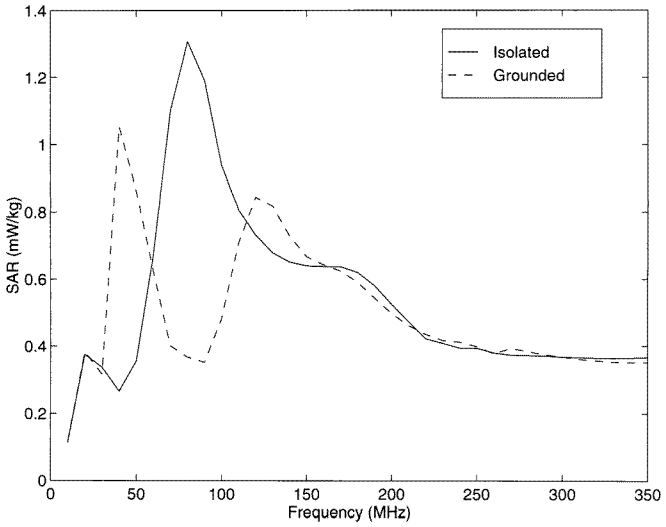

Figure 7. The mass-averaged SAR in the torso under grounded conditions. $D_{\mathrm{inc}} = 1$ mW cm^{-2}.

body through the constricted volume of the neck thus concentrating them (i.e. increasing the current density) and as a result increasing the SAR.

We have used an enhancement factor (defined in equation (2)) to show the effect of the larger power absorption in the head and neck at resonance. Table 5 shows these values together with the head and neck averaged SAR at 207 MHz.

When the model is grounded significant changes occur with respect to the frequency and magnitude of the head resonances. Furthermore a new resonant frequency is found to exist close to 120 MHz, both for the anatomically based model as well as the approximation model. This is interesting since a similarly high absorption is not observed around this frequency under isolated conditions. Observation of the power absorption in the torso (defined between heights 0.85 m, and 1.55 m, given in figure 7), shows a single resonance under isolated conditions, whereas when the model is grounded two resonances occur. It would appear that the whole body resonance and the torso resonance overlap in the isolated condition. However, when the model is grounded these are separated with the frequency of the whole body resonance lowered from 79 MHz for the isolated case to 48 MHz. It would further appear that the torso resonance does not change significantly when the model is grounded and thus becomes discernible as an individual resonance.

The first head and neck resonance, at 79 MHz for the isolated case, has moved to 48 MHz by virtue of the fact that this is a part of the whole body resonance, which has also moved (figure 3(*b*)). The main head and neck resonance (highest in magnitude) has not changed significantly, moving from 207 MHz to 193 MHz (figure 3(*b*)). The power absorption at 193 MHz is highest in the head and neck alone under grounded conditions, and there is not similar peak in the power absorbed in the torso. It has also been observed that the power absorbed in the head and neck, at each of the resonant frequencies, is less than that for the isolated condition. From the layer-averaged SAR distributions at each of these three frequencies (figures 8(*a*)–8(*c*)) it can be seen that from 79 MHz to 113 MHz there is a reduction in the power absorbed in the legs and ankles, and at 193 MHz the highest power absorption is in the head and neck. The SAR distribution in the head and

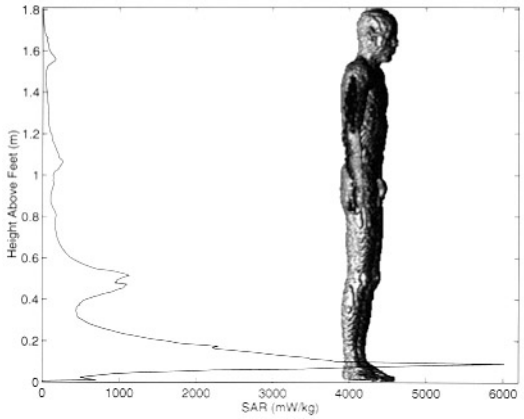

(*a*)

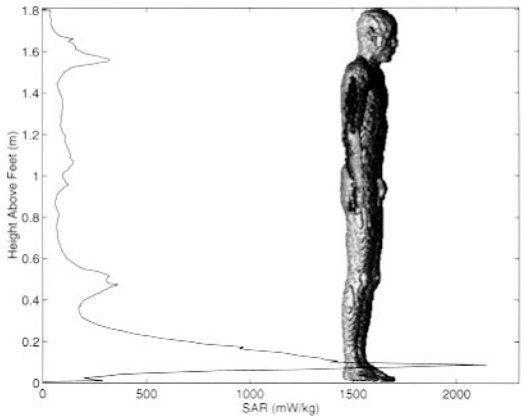

(*b*)

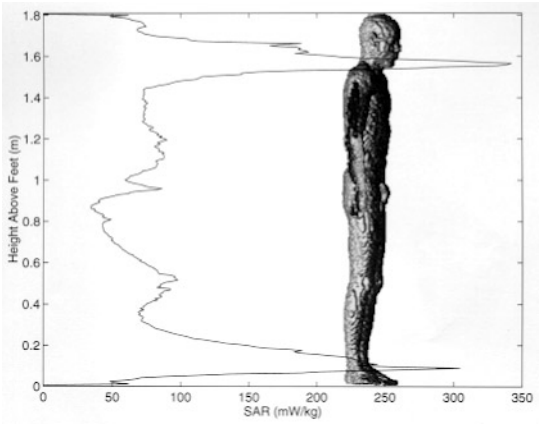

(*c*)

Figure 8. The layer-averaged SAR for the 6 mm heterogeneous man model at 48 MHz (*a*), 113 MHz (*b*) and 193 MHz (*c*). $D_{\mathrm{inc}} = 1$ mW cm^{-2}.

neck region at the new resonant frequency of 193 MHzis very similar to that for resonance under isolated conditions of the model previously shown in figure 6.

Table 5. Enhancement factors and head and neck averaged SAR for 6 mm whole body model and the scaled 5- and 10-year-old child models. Shown in parentheses are the resonant frequencies for which the various parameters have been calculated.

	1.974 × 1.974× 3.0 mm adult model	5.922 × 5.922× 6.0 mm adult model	Scaled 10-year-old child model	Scaled 5-year-old child model
Whole-body averaged SAR —isolated[a]	282.4 (78 MHz)	283.0 (78 MHz)	354.7 (104 MHz)	377.4 (126 MHz)
Whole-body averaged SAR —grounded[a]	357.5 (47 MHz)	359.0 (47 MHz)	370.3 (65 MHz)	383.7 (73 MHz)
Whole body enhancement factor *S* —isolated[a]	3.88 (78 MHz)	3.87 (78 MHz)	3.89 (104 MHz)	3.58 (126 MHz)
Whole body enhancement factor *S* —grounded[a]	4.91 (78 MHz)	4.92 (47 MHz)	4.1 (65 MHz)	3.63 (73 MHz)
Head and neck averaged SAR (mW kg^{-1}) —isolated[b]	220.4 (207 MHz	227.6 (207 MHz)	246.8 (263 MHz)	291.0 (322 MHz)
Head and neck averaged SAR (mW kg^{-1}) —grounded[b]	169.0 (193 MHz)	182.4 (193 MHz)	219.7 (244 MHz)	235.5 (325 MHz)
Head and neck enhancement factor *S* —isolated[b]	3.38 (207 MHz)	3.27 (207 MHz)	3.26 (263 MHz)	3.13 (322 MHz)
Head and neck enhancement factor *S* —grounded[b]	2.57 (193 MHz)	2.62 (193 MHz)	2.90 (244 MHz)	2.53 (325 MHz)

[a] When whole body is resonant.
[b] When head and neck are resonant.

The power absorption in both the brain and the eyes has been considered under both isolated and grounded conditions (figures 9(*a*) and 9(*b*) respectively). As would be expected, the power absorption in these organs has a similar pattern to that of the head and neck.

Additional comparisons have been made for organ-averaged SAR values from simulations using the 2 mm and 6 mm resolution whole body models. Two simulations were carried out at 207 MHz using the 2 mm whole body model and the 6 mm whole body model (both isolated). Table 6 shows that that for most of the tissues shown there is only a small difference between the two models. However, in the case of the smaller organs such as the eye lens there is a more significant difference. This arises due to the fact that when the cells from the higher-resolution model were combined to produce the lower-resolution model, tissues with small dimensions were lost or reduced in size. It is fair to say that for the purposes of this work the lower-resolution anatomically based model was satisfactory; however, if a detailed study of the effects of EM fields upon individual tissues (such as the eyes), was made, then the use of the higher-resolution model would be desirable.

Table 6. A comparison of the tissue-averaged SAR (at 207 MHz) for the 2 mm and 6 mm anatomically based whole body models.

	Tissue-averaged SAR (mW kg^{-1})		
	2 mm adult model	6 mm adult model	Difference (%)
Whole-body averaged SAR	104.0	99.6	4.5
Head and neck averaged SAR	20.4	227.6	3.2
Muscle	154.3	153.7	0.3
Fat	33.4	34.8	4.1
Skin	153.9	70.8	117.4
Nerve	133.0	138.5	3.9
Intestine	48.8	53.8	9.2
Spleen	27.7	23.5	17.8
Pancreas	22.2	16.8	31.6
Heart	52.1	53.4	2.5
Blood	176.9	180.4	2.0
Parotid gland	573.6	434.6	32.0
Liver	34.2	32.3	6.1
Kidney	22.8	23.9	4.5
CSF	245.5	252.1	2.6
Eye—humour	400.1	408.1	2.0
Eye—sclera	287.0	274.7	4.5
Eye—lens	216.5	304.4	28.9
Stomach	46.9	45.2	3.8
Prostate	5.02	4.47	12.4
Testicle	34.6	36.2	4.5
Pineal gland	171.1	171.1	0.0
Pituitary gland	440.8	572.4	23.0
Brain	142.7	147.4	3.2

5. 5-year-old and 10-year-old children

Simulations carried out in a similar manner for scaled models of 5- to 10-year-old children have produced results in line with those expected. Here it should be noted that scaling an adult human model does not produce a truly accurate model of a child and there can be errors in the weights of some tissues (i.e. not all the organs scale at the same rate with respect to age). However, it should also be noted that the results presented here correspond to properties which are based on the general dimensions of the body and not specific organs and thus, as the height and weight of the scaled models of 5- and 10-year-old children are in line with expected values, their use can be justified. Although the power absorption spectrum has a similar shape, the resonant frequencies have been shifted. As seen in table 5, these frequencies are dependent upon the height of the model, for both the whole body and the head and neck region. In the case of the 10-year-old child this can be observed when comparing figure 10(*a*) with figure 3(*a*), for the isolated condition and figure 10(*b*) and figure 3(*b*) for the grounded condition. Similar results are given for the 5-year-old child (figures 11(*a*) and 11(*b*)). As would be anticipated, this frequency change is predicted by the change in height between the adult and the 5- and 10-year-old children. The 10-year-old child has a height of 1.41 m and the adult a height of 1.81 m. The ratio of frequencies for the grounded conditions is 244 MHz to 193 MHz or 1.26 and the ratio in heights is 1.28. Similar observations can be made for the 5-year-old child. As would also be expected, a

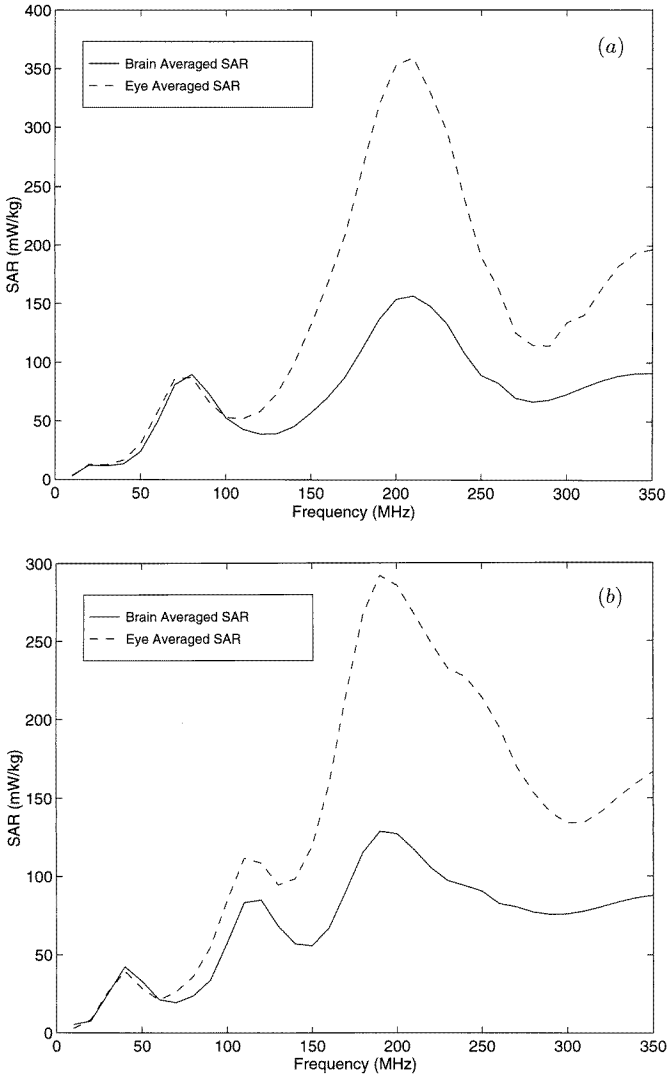

Figure 9. Mass-averaged SAR in the brain and eye under isolated (*a*) and grounded (*b*) conditions. $D_{\mathrm{inc}} = 1$ mW cm^{-2}.

reduction in the size of the model for the 10- and 5-year-old children results in an increase in whole body and head and neck averaged SAR values (table 5).

6. Conclusions

In this paper we have determined the frequencies at which the whole body and head and neck resonances occur, in models of the adult male and 10- and 5-year-old children. For the model of the adult, the head and neck averaged SAR has peak values of 227.6 mW kg^{-1} and 184 mW kg^{-1}, for isolated and grounded model resonant frequencies of 207 MHz and 193 MHz, respectively. These SAR values equate to absorption cross section enhancement

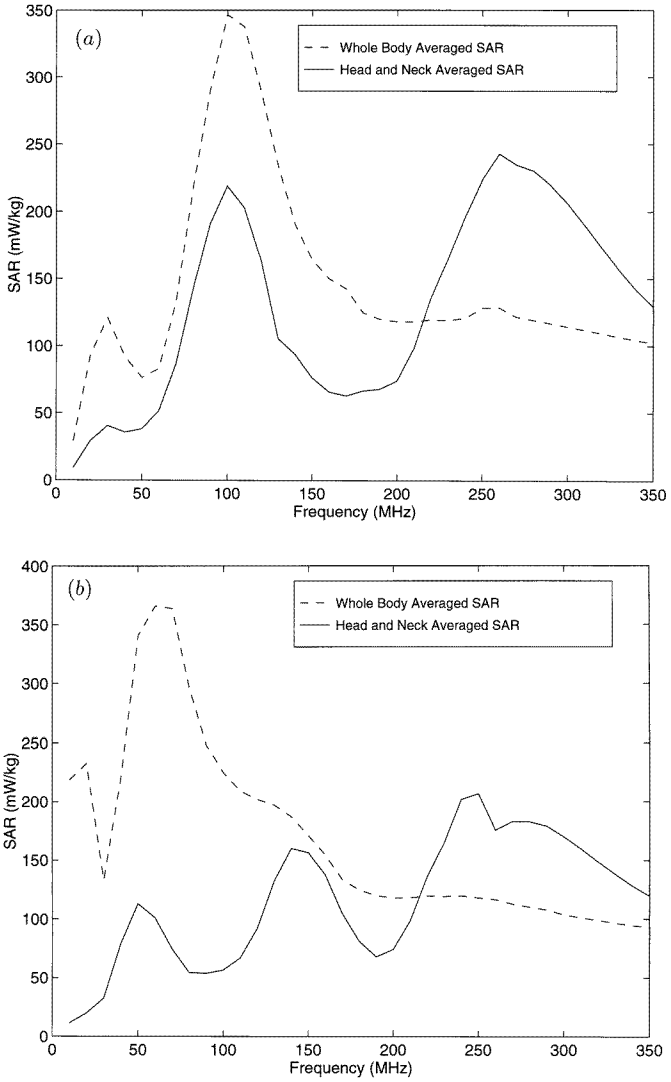

Figure 10. The mass-averaged SAR in the head and neck and whole body of the scaled 10-year-old child model under isolated (*a*) and ground (*b*) conditions. $D_{\mathrm{inc}} = 1$ mW cm^{-2}.

factors of 3.27 and 2.62 respectively, which demonstrate that a disproportionate amount of power is absorbed in the head and neck at these frequencies. Additionally it was observed that under isolated conditions two clear resonant frequencies could be observed for the head and neck, whereas under grounded conditions three resonances were observed. The additional resonance under grounded conditions was found to be a partial body resonance associated with the torso.

We have also demonstrated the use of a high-resolution model of the human body ($1.974 \times 1.974 \times 3.0$ mm), together with the introduction of methods to carry out simulations with the large quantities of data produced by such models. Although the use of this finer resolution is not strictly necessary for computations of the volume-averaged SARs used in

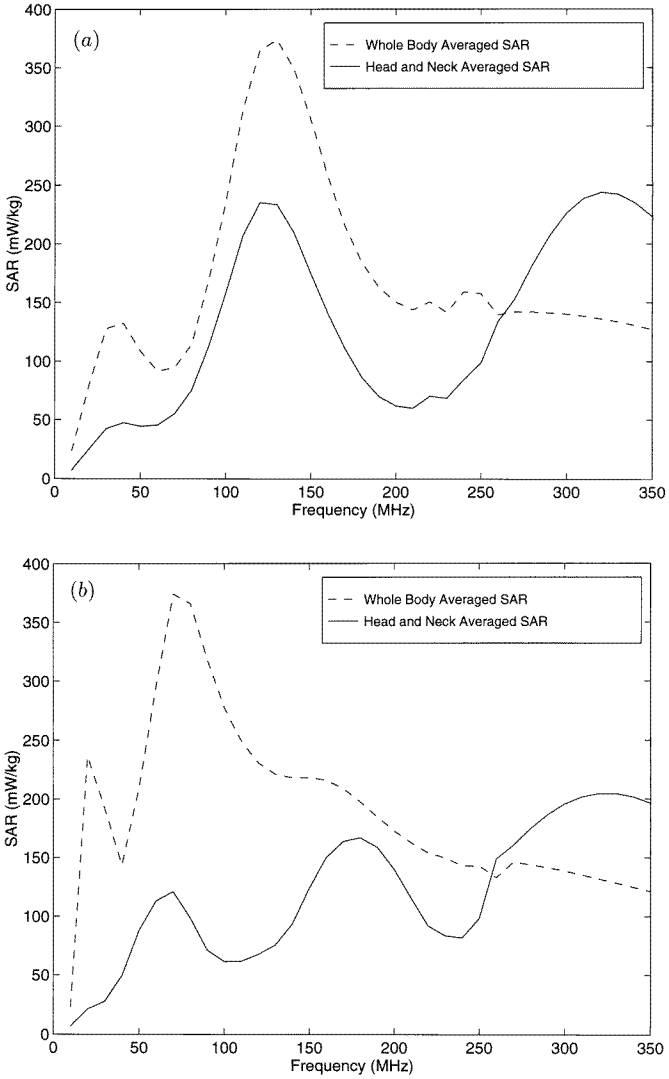

Figure 11. The mass-averaged SAR in the head and neck and whole body of the scaled 5-year-old child model under isolated (a) and grounded (b) conditions. $D_{\mathrm{inc}} = 1$ mW cm^{-2}.

this paper, it is clear from the comparisons of tissue-averaged SARs between this and the lower-resolution model that the study of power absorption in smaller organs would benefit from the higher-resolution model.

Acknowledgments

The authors acknowledge many helpful discussions with Dr John A D'Andrea. This research group was sponsored by the Naval Medical Research and Development Command under work unit 61153N MRO 4101.001-1603.

References

Berntsen S and Hornsleth S N 1994 Retarded time absorbing boundary conditions *IEEE Trans. Antennas Propagation* **42** 1059–64

Furse C M, Cui Y, Lazzi G and Gandhi O P 1997 Use of PML boundary conditions for wireless telephone simulations *Microwave Opt. Technol. Lett.* **15** (2) 95–8

Dimbylow P J 1997 FDTD calculations of the whole-body averaged SAR in an anatomically realistic voxel model of the human body from 1 MHz to 1 GHz *Phys. Med. Biol.* **42** 479–90

Gabriel C 1996 Compilation of the dielectric properties of body tissues at RF and microwave frequencies *Final Technical Report Occupational and Environmental Health Directorate AL/OE-TR-1996-0037* (Brooks Air Force Base, TX: RFR Division)

Gandhi O P, Gu Y, Chen J Y and Bassen H I 1992 Specific absorption rates and induced current distributions in an anatomically based human model for plane-wave exposures *Health Phys.* **63** 281–90

Guy A W, Chou C K and Neuhaus B 1984 Average SAR and SAR distribution in man exposed to 450 MHz radio frequency radiation *IEEE Trans. Microwave Theory Tech.* **32** 752–63

Hagmann M J, Gandhi O P and Durney C H 1979 Numerical calculation of electromagnetic energy deposition for a realistic model of man *IEEE Trans. Microwave Theory Tech.* **27** 804–9

IRCP 1975 Report of the task group on reference man *IRCP Publication 23* (Oxford: Pergamon)

Stuchly S S, Kreszewski A, Stuchly M A, Hartsgrove G W and Spiegel R J 1988 RF energy deposition in a heterogeneous model of man; far-field exposures *IEEE Trans. Biomed. Eng.* **35** 179–86

Taflove A 1995 *Computational Electrodynamics: The Finite-Difference Time-Domain Method* (Dedham, MA: Artech House)

Tinniswood A D, Furse C M and Gandhi O P 1998 Computations of SAR distributions for two anatomically-based models of the human head using CAD files of commercial telephones and the parallelized FDTD code *IEEE Trans. Antennas Propag.* **46** 829–33